Structure of an E6AP-UbcH7 Complex: Insights into Ubiquitination by the E2-E3 Enzyme Cascade

Lan Huang,[1] Elspeth Kinnucan,[1] Guangli Wang,[3] Sylvie Beaudenon,[3] Peter M. Howley,[4] Jon M. Huibregtse,[3] Nikola P. Pavletich[1,2]*

The E6AP ubiquitin-protein ligase (E3) mediates the human papillomavirus-induced degradation of the p53 tumor suppressor in cervical cancer and is mutated in Angelman syndrome, a neurological disorder. The crystal structure of the catalytic hect domain of E6AP reveals a bilobal structure with a broad catalytic cleft at the junction of the two lobes. The cleft consists of conserved residues whose mutation interferes with ubiquitin-thioester bond formation and is the site of Angelman syndrome mutations. The crystal structure of the E6AP hect domain bound to the UbcH7 ubiquitin-conjugating enzyme (E2) reveals the determinants of E2-E3 specificity and provides insights into the transfer of ubiquitin from the E2 to the E3.

Ubiquitin-dependent proteolysis is an important regulatory mechanism involved in diverse cellular processes such as cell cycle control and signal transduction (*1, 2*), and deregulation of targeted proteolysis has been implicated in several human diseases (*3*). The cellular E6AP protein is a ubiquitin-protein ligase that mediates the human papillomavirus (HPV) E6 protein-induced ubiquitination and subsequent degradation of the p53 tumor suppressor (*4, 5*), an event that contributes to the development of more than 90% of cervical carcinomas. E6AP is also involved in Angelman syndrome (AS), where inherited mutations, deletions, or other alterations in E6AP cause severe motor dysfunction and mental retardation (*6, 7*). It is unknown which substrates are critical for AS, but the proteins that E6AP ubiquitinates include the activated forms of several Src family protein kinases (*8*), the human Rad23 homolog HHR23A (*9*), and the MCM-7 protein implicated in chromosomal replication (*10*). In the absence of HPV E6, E6AP does not ubiquitinate p53 (*4, 5, 11*).

Ubiquitination reactions involve the successive action of E1, E2, and E3 activities (*12*). The E1 (ubiquitin-activating) enzyme, in an adenosine triphosphate (ATP)–dependent reaction, activates ubiquitin by forming a thioester bond at its active-site cysteine with the COOH-terminus of ubiquitin. Ubiquitin is then transferred to the active-site cysteine of E2 (ubiquitin-conjugating) enzymes, maintaining a thioester linkage. E3s, also known as ubiquitin-protein ligases, are minimally defined as additional proteins or protein complexes necessary for the recognition and ubiquitination of specific substrates, and these appear to be a functionally diverse set of activities. E6AP belongs to the hect (homologous to E6AP COOH-terminus) class of E3s, which has at least 20 members in humans (*13*). The hect E3s are so far unique among the known classes of E3s in that they form a ubiquitin-thioester intermediate and directly catalyze substrate ubiquitination (*14*). The other E3 classes, including the Skp1-Cullin-F box (SCF) complexes and the anaphase-promoting complex (APC), have not been shown to form thioester intermediates with ubiquitin (*12*).

Hect E3s share a conserved ~40-kD COOH-terminal catalytic domain, the hect domain, that has at least four biochemical activities: (i) it binds specific E2s; (ii) it accepts ubiquitin from the E2, forming a ubiquitin-thioester intermediate with its active-site cysteine; (iii) it transfers ubiquitin to the ε-amino groups of lysine side chains on the substrate by catalyzing the formation of an isopeptide bond; and (iv) it transfers additional ubiquitin molecules to the growing end of the multi-ubiquitin chain (*12, 13, 15*). The NH_2-terminal sequences of hect E3s are not conserved and contain the primary determinants for specific substrate recognition. The recognition of HPV E6 and p53 requires a ~200-residue E6AP region NH_2-terminal to the hect domain (*5*).

E2s form a closely related family of proteins, with about 30 E2s known in humans. They contain a 150–amino acid conserved catalytic core but can have NH_2- or COOH-terminal extensions, or both (*16*). E2s can be divided into subfamilies according to their specificity for different E3 classes. The E2 subfamily that functions with the hect class of E3s includes the human UbcH5, UbcH7, and UbcH8. Individual E2s within this subfamily display preference for specific hect E3s as well, and this is due to the specificity in the binding of the E2 to the hect domain (*13, 17–19*).

To begin to understand how the hect E3 activities are organized, coordinated, and contribute to specificity, we have determined the 2.8 Å structure (*20, 21*) of the hect domain of human E6AP (residues 495 to 852) and the 2.6 Å structure (*20, 22*) of this domain bound to the human UbcH7 ubiquitin-conjugating enzyme.

Overall structure of the E6AP hect domain–UbcH7 complex. The complex has a U-shaped structure, with the E6AP hect domain representing the base and one side and UbcH7 representing the other side (Fig. 1, A and B, and Table 1). The hect domain consists of two lobes that pack loosely across a small interface and are connected by a three-residue hinge (residues 738 to 740). The larger NH_2-terminal lobe (residues 495 to 737) has a mostly α-helical structure with an elongated shape. The smaller COOH-terminal lobe (residues 741 to 852) has an α/β structure and contains the catalytic Cys^{820} that forms the thioester bond with ubiquitin.

At the junction of the two lobes, there is a broad cleft that contains Cys^{820} at its base (Fig. 1, A and B). The N-lobe portion of the cleft contains mostly polar and charged residues and has an overall negative charge. Residues contributing to this feature are generally conserved among hect family members. The C-lobe portion of the cleft contains a hydrophobic patch consisting of conserved residues that are partially exposed to solvent.

UbcH7, which consists of little more than the conserved 150-residue E2 catalytic core, has an α/β structure similar to the structures of other E2s (*23*). UbcH7 binds in a large hydrophobic groove on the N lobe of the E6AP hect domain, using loops at one end of its β sheet and a portion of its NH_2-terminal α helix. A phenylalanine (Phe^{63}), conserved only in the hect-specific E2 subfamily (*24*), binds in the center of the hydrophobic groove of the hect domain. The overall structure of the hect domain does not change upon UbcH7 binding (*25*).

The E2-binding groove on the E6AP hect domain consists of residues that are only moderately conserved but maintain their hydrophobic character in other hect E3s (Fig. 1C). The groove occurs in a part of the E6AP

[1]Cellular Biochemistry and Biophysics Program, [2]Howard Hughes Medical Institute, Memorial Sloan-Kettering Cancer Center, New York, NY 10021, USA. [3]Department of Molecular Biology and Biochemistry, Rutgers University, Piscataway, NJ 08855, USA. [4]Department of Pathology, Harvard Medical School, Boston, MA 02115, USA.
*To whom correspondence should be addressed.

N-lobe structure that appears to be an 80-residue subdomain, having its own hydrophobic core and connected to the rest of the N lobe through a mostly polar interface and two linkers (residues 621 to 622 and 702 to 704). The E6AP and UbcH7 active-site cysteine side chains are 41 Å apart and have an open line of sight between them.

Catalytic cysteine maps to the interface between the N and C lobes. Cys^{820} is positioned near the center of a four-residue loop between the S9 and S10 β strands on the C lobe. This loop, hereafter termed the active-site loop, is nestled next to the N lobe and also interacts with it (Figs. 1 and 2). All four of the active-site loop residues (Thr^{819}, Cys^{820}, Phe^{821}, and Asn^{822}) have roles in interdomain packing. Thr^{819} and Asn^{822} form hydrogen bonds with the N-lobe residues and also pack with the rest of the C lobe (Fig. 2). Phe^{821} makes van der Waals contacts with the N-lobe Gly^{546} (Fig. 2). The thiol group of the catalytic Cys^{820} is partially exposed to solvent and is in a mixed hydrophobic and polar environment. It makes van der Waals contacts with the face of the adjacent Phe^{821} phenyl group, and is 4.6 Å from the Glu^{550} carboxylate group and 6.7 Å from the His^{818} side chain (Fig. 2). The side chains of Glu^{550} and His^{818} could, in principle, adopt conformations that would allow them to interact with the Cys^{820} thiol group (Fig. 2).

The contacts between the active-site loop and the N lobe are separated from the N-C lobe hinge by a solvent channel ~5 Å across (Fig. 2). The N-C hinge contains the remainder of the noncovalent contacts between the two lobes, and these involve residues that are partially conserved (Asn^{603}, Ile^{605}, Pro^{793}, and Val^{794}; Fig. 2).

Structure and mutagenesis of the cleft surrounding the catalytic cysteine. The active-site loop is positioned at the base of a broad, shallow cleft (~20 Å wide by ~5 Å deep) that is formed by structural elements from both the N and C lobes (Fig. 3A). A comparison of 18 hect domain sequences from different species, including all five yeast hect E3s, indicates that this broad cleft is the best conserved portion of the molecular surface (Fig. 3A). The highest conservation maps to the active-site loop, to a flanking acidic patch on the N lobe, and to a flanking hydrophobic patch on the C lobe (Fig. 3B).

In the active-site loop, Thr^{819} and Asn^{822} are highly conserved, whereas Phe^{821} and His^{818} preceding this loop are moderately conserved. Mutation of Thr^{819}, Asn^{822}, or Phe^{821} to Ala reduced the ability of the hect domain to form the ubiquitin thioester intermediate in our in vitro assay by ~70% (*26*), suggesting that the contacts made by the active-site loop at the N-C lobe interface are important for this activity. The H818A mutation caused a reduction of more than 95% (*26*); as His^{818} has no apparent structural

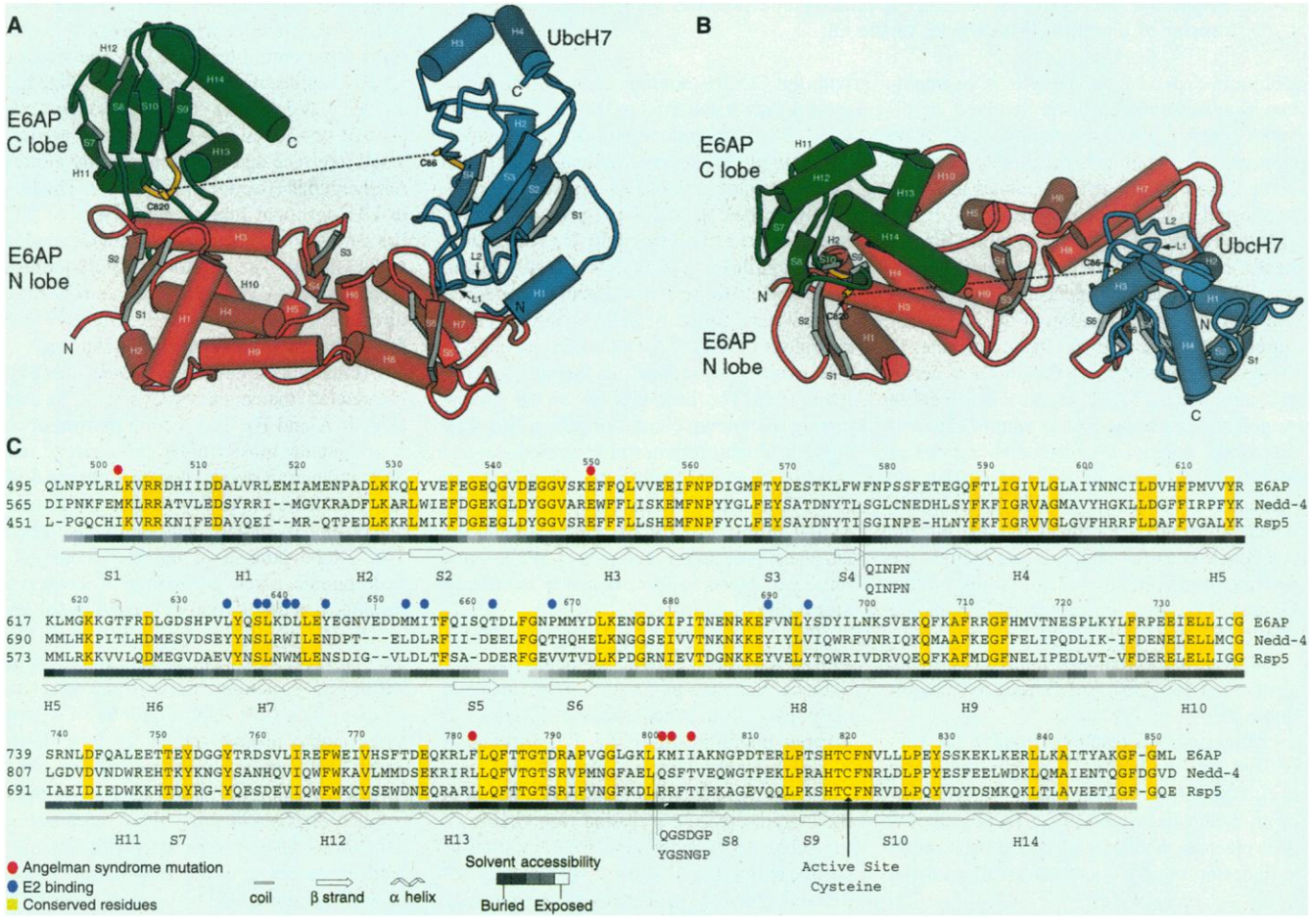

Fig. 1. The E6AP hect domain–UbcH7 complex forms a U-shaped structure. (**A** and **B**) Orthogonal views of the overall structure of the complex. The E6AP hect domain N lobe (consisting of 12 α helices and six β strands), C lobe (six α helices and four β strands), and UbcH7 (four α helices and four β strands) are colored in green, red, and cyan, respectively. The two active-site loops are colored yellow. The hect-binding loops of UbcH7 are labeled L1 (residues 57 to 65) and L2 (residues 95 to 100). The UbcH7 active-site loop consists of residues 70 to 101. The dotted line indicates the open line of sight between the active-site cysteines of E6AP and UbcH7. [Prepared with the programs MOLSCRIPT and RASTER3D (*42*).] (**C**) Alignment of the hect domain sequences of human E6AP, human Nedd4, and yeast Rsp5. Secondary structure elements are indicated. Sequence identity is shown in yellow. Cyan dots mark E6AP residues that contact UbcH7; red dots represent residues mutated in Angelman syndrome. Shaded squares below each residue describe the relative solvent exposure of a residue in a monomer of E6AP.

role, this finding suggests that it may participate in catalysis.

The highest conservation on the N-lobe portion of the cleft surface maps to Arg^{506}, Glu^{539}, and Glu^{550}, which together form a solvent-exposed salt-bridge network adjacent to the catalytic cysteine and to Asp^{607} (Fig. 3B). Mutation of any one of these four conserved residues on the N lobe reduced ubiquitin-thioester formation by more than 90% (*26*), indicating that the N-lobe portion of the cleft is also needed for this activity.

The highest conservation on the C-lobe hydrophobic patch maps to Phe^{785}, Leu^{814}, Pro^{815}, Ala^{842}, and Phe^{849}. With the exception of Phe^{849}, these residues make van der Waals contacts with each other and are only partially solvent-exposed. Phe^{849} is solvent-exposed and occurs in the partially disordered three-residue COOH-terminal segment of the protein. Previous studies have shown that deletion of the last six residues of E6AP, including Phe, eliminates isopeptide bond formation between ubiquitin and the substrate protein without substantially affecting the formation of the ubiquitin-thioester intermediate (*27*). This result implicates residues in the C lobe as being critical for the catalysis of isopeptide bond formation.

Angelman syndrome mutations. Most of the AS-associated missense and single amino acid insertion or deletion mutations in the hect domain map to the catalytic cleft. The E550L mutation (*28*) maps to the conserved salt-bridge network on the N-lobe portion of the cleft (Fig. 3B), and, as discussed above, the E550A mutation reduces thioester formation by more than 90% (*26*). L502P (*28*) also maps to the N-lobe portion of the cleft, to a hydrophobic core residue (Fig. 3B). The I804K (*29*), F782del (*29*), and M802ins (*30*) mutations map to the hydrophobic core of the C lobe, and these mutations would be predicted to destabilize the folded state of the C lobe. The K801del mutation (*31*) occurs immediately before the S8 strand, adjacent to the active-site loop, and the structure suggests that this deletion mutation would affect the local structure in the vicinity of the active-site loop.

Other functions have been attributed to E6AP, but an analysis of AS mutations showed a clear correlation between the loss of the ubiquitin-protein ligase function of E6AP and AS (*32*). Our observation that many of the AS mutations map to the catalytic cleft solidifies the role of the E3 activity of E6AP in the etiology of AS.

Structure of the E6AP hect domain–UbcH7 interface. UbcH7 has an elongated α/β structure that consists of a four-stranded β sheet and four α helices (Fig. 1, A and B) (*23*). The UbcH7 active-site cysteine (Cys^{86}) is positioned on the side of the sheet in the middle of a 30–amino acid loop (Fig. 1A). One end of the elongated UbcH7 structure binds to a V-shaped hydrophobic groove on the N lobe of E6AP, burying a total of 1800 $Å^2$ of surface area. The E6AP groove consists of two antiparallel helices that form one side, two antiparallel β strands that form the other side, and a loop that caps one end (Fig. 1, A and B). The portion of UbcH7 that binds E6AP consists of the L1 and L2 loops and the H1 helix (Figs. 1A and 4A). Among these, the L1 loop contributes the most extensive E6AP contacts (*33*). These are augmented by contacts from the L2 loop and by a few contacts from the H1 helix (*34*) (Figs. 1 and 4).

The most critical contacts to E6AP are made by Phe^{63} of the UbcH7 L1 loop. The Phe^{63} side chain binds in the central, deepest portion of the E6AP groove and makes van der Waals contacts with six hydrophobic and aromatic E6AP side chains (Fig. 4, B and C)

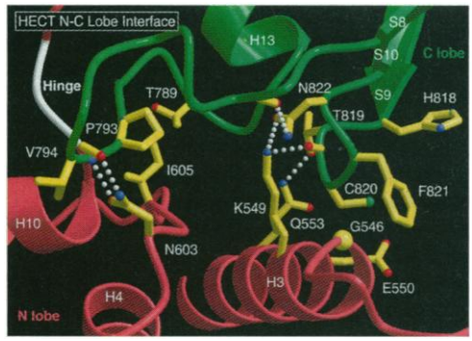

Fig. 2. The E6AP catalytic cysteine (Cys^{820}) maps to the interface between the N and C lobes of the hect domain. Residues of the active-site loop and those that make N-C lobe contacts are shown in yellow. N and C lobes are colored red and green, respectively. The hinge region (residues 738 to 740) between the N and C lobes is colored white. White dashed lines indicate hydrogen bonds; red atoms, oxygen; blue, nitrogen; green, sulfur.

Table 1. Statistics from the crystallographic analysis.

Data set	E6AP native	E6AP SeMet λ1	E6AP SeMet λ2	E6AP SeMet λ3	E6AP-UbcH7 native
Wavelength (Å)	1.54	0.9793	0.9789	0.9678	1.000
Beamline	–	NSLS-X4a	X4a	X4a	ALS(5.0.2)
Resolution (Å)	2.8	3.2	3.2	3.2	2.6
Observations	127,891	158,014	156,174	157,543	106,238
Unique reflections	35,446	23,561	23,553	23,622	42,425
Data coverage (%)	97.7	96.6	96.6	96.6	89.8
R_{sym} (%)	5.7	7.1	7.6	7.3	5.5
MAD analysis (20.0 to 3.3 Å)					
Phasing power	–	1.21	0.55	0.84	
R_{cullis}	–	–	0.93	0.86	
$R_{cullis\ (ano)}$	–	0.75	0.72	0.76	

Refinement statistics

Data set	Resolution (Å)	Reflections ($\|F\| > 2\sigma$)	Total atoms	Water atoms	*R* factor (%)	R_{free} (%)	RMSD Bonds (Å)	RMSD Angles (°)	RMSD *B* factor ($Å^2$)
E6AP	15.0–2.8	32,190	10,413	0	22.6	28.5	0.012	1.856	2.4
E6AP-UbcH7	15.0–2.6	36,839	11,754	359	24.2	28.6	0.011	1.707	2.2

$R_{sym} = \Sigma_h\Sigma_i|I_{h,i} - I_h|/\Sigma_h\Sigma_i I_{h,i}$ for the intensity (I) of i observations of reflection h. Phasing power = $\langle F_{hi}\rangle/E$, where $\langle F_{hi}\rangle$ is the root mean square heavy atom structure factor and E is the residual lack-of-closure error. R_{cullis} is the mean residual lack-of-closure error divided by the dispersive or anomalous difference. *R* factor = $\Sigma||F_{obs} - F_{calc}||/\Sigma|F_{obs}|$, where F_{obs} and F_{calc} are the observed and calculated structure factors, respectively. Figure of merit = $|F(hkl)_{best}|/|F(hkl)|$. R_{free} = *R* factor calculated using 5% of the reflection data chosen randomly and omitted from the start of refinement. RMSD, root mean square deviations from ideal geometry and root mean square variation in the *B* factor of bonded atoms.

(*33*). The Phe^{63} backbone carbonyl group forms hydrogen bonds with the side chain of the conserved E6AP Ser^{638}. Additional contacts from the UbcH7 L1 loop are made by the side chains of Ala^{59}, Pro^{62}, and Glu^{60} and the backbone carbonyl of Ala^{59} (Fig. 4, A to C) (*33*).

The UbcH7 L2 loop is positioned adjacent to the L1 loop and binds at the entrance of the E6AP groove (Fig. 4D). The L2 loop Pro^{97} and Ala^{98} make van der Waals contacts to hydrophobic and polar E6AP residues (*34*), whereas Lys^{96} and Lys^{100} form hydrogen bonds with the side chain of the E6AP Asp^{641} and the backbone carbonyl of Asp^{652}, respectively (Fig. 4D).

E2-E3 specificity. The central role of Phe^{63} in binding the hect domain, considered together with the conservation of Phe^{63} in E2s known to support hect domain–mediated ubiquitination in vitro (UbcH5, UbcH7, and UbcH8) but not in E2s that function with non-hect E3s (Fig. 4A), suggests that a Phe at this position may be the primary determinant of the specificity of an E2 for the hect family of E3s. This is supported by a recent study where mutation of the corresponding Phe in UbcH5 to Asn eliminated the ability of UbcH5 to function with the hect E3 Rsp5 in vitro (*24*). Conversely, introduction of a Phe at this position in the non-hect E2 UbcH1 allowed for partial function of a chimeric UbcH1/UbcH5 with Rsp5 (*24*). We thus refer to the L1 loop as the specificity loop to reflect the proposed role of Phe^{63} in hect specificity.

Several studies have indicated that individual E2s from the hect-specific subfamily may have preferences for different hect E3s. In a yeast two-hybrid assay, UbcH7 and UbcH8 interacted with E6AP but not with Rsp5, and conversely, UbcH5 interacted with Rsp5 but not with E6AP (*19*). This preference was also reflected in the efficiency of ubiquitin-thioester intermediate formation in vitro (*13*). This could be due, in part, to the contacts made by the L2 loop, which is more variable than the L1 specificity loop within the hect-specific E2 subfamily (Fig. 4A). The two Lys residues (Lys^{96} and Lys^{100}) of the UbcH7 L2 loop are conserved in UbcH8 but not in UbcH5, where they are Ser and Thr, respectively (Fig. 4A). The residues and structural elements of E6AP that are contacted by these UbcH7 Lys side chains differ in Rsp5. The E6AP Asp^{641} is replaced by a Trp in Rsp5, and the E6AP Asp^{652} backbone carbonyl group is in a region that has a two-residue deletion in Rsp5 (Fig. 1C).

Transfer of ubiquitin. The transfer of ubiquitin from the E2 to the hect E3 likely proceeds through a nucleophilic attack on the E2-ubiquitin thioester bond by the hect active-site cysteine. This would require the active-site cysteines of the E2 and the hect E3 to be in close proximity. However, in our structure the two thiol groups are separated by 41 Å. It is not clear why the E2 and E3 active sites are far apart, but this would, in principle, make the E2 active site more accessible to the E1 enzyme, and allow for the reloading of the E2 with ubiquitin while it is still bound to the E3. However, it has not yet been determined whether the E2 remains associated with the hect domain during each enzymatic cycle.

The juxtaposition of the E2 and E3 active sites during ubiquitin transfer appears to require a large conformational change in the complex. This may involve a change in the relative orientation of the N and C lobes, a conformational change in the N-lobe structure between the E2-binding subdomain and the C-lobe attachment site, or a conformational change in the 30-residue E2 loop that harbors the catalytic cysteine. It is conceivable that a different conformation of the E2-E3 complex, where the two active sites are juxtaposed, also exists in solution. Alternatively, a conformational change in the complex may be triggered by the E2-linked ubiquitin, and this could be mediated by interactions between ubiquitin and the hect domain. Either the N-lobe acidic patch or the C-lobe hydrophobic patch of the hect cleft could be a possible ubiquitin interaction site, as ubiquitin contains both a basic patch and a hydrophobic patch (*35*, *36*) near its COOH-terminus.

The structures of the E6AP hect domain and of its complex with UbcH7 provide the first views of an E3 enzyme and of an E2-E3 complex. These structures, in conjunction with mutagenesis data, provide insights into the mechanism of ubiquitin transfer and the specificity in the E2-E3 enzyme cascade.

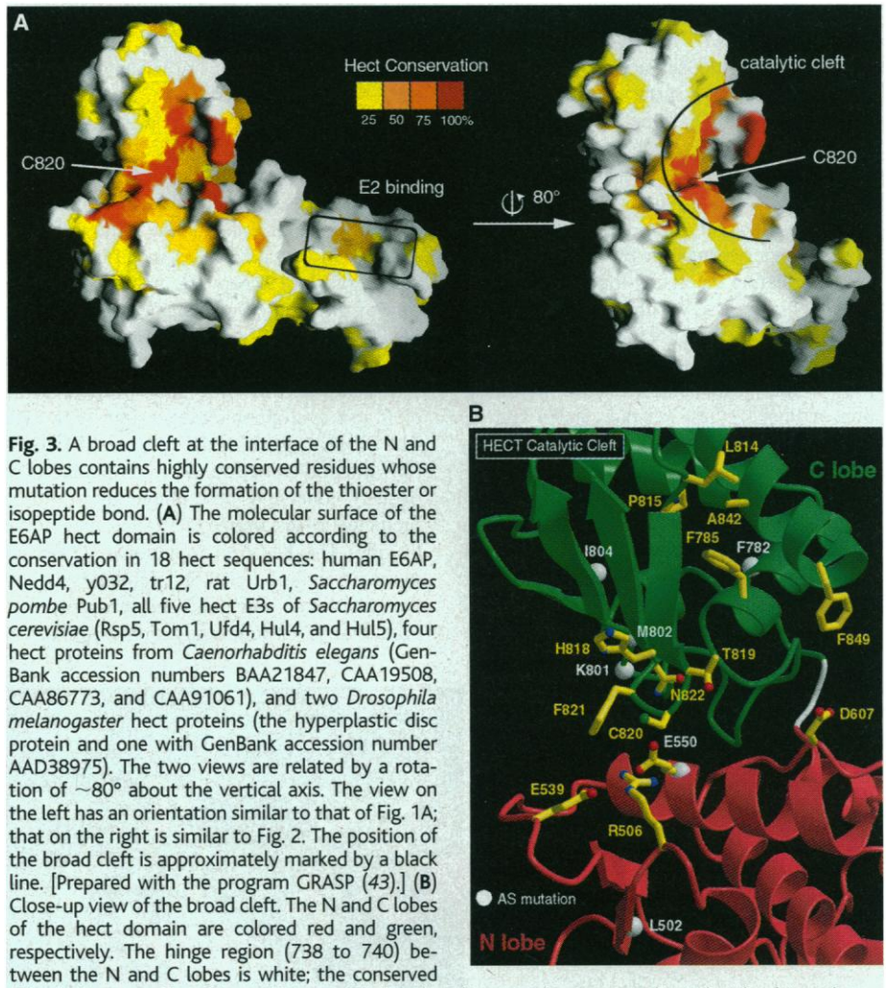

Fig. 3. A broad cleft at the interface of the N and C lobes contains highly conserved residues whose mutation reduces the formation of the thioester or isopeptide bond. (**A**) The molecular surface of the E6AP hect domain is colored according to the conservation in 18 hect sequences: human E6AP, Nedd4, y032, tr12, rat Urb1, *Saccharomyces pombe* Pub1, all five hect E3s of *Saccharomyces cerevisiae* (Rsp5, Tom1, Ufd4, Hul4, and Hul5), four hect proteins from *Caenorhabditis elegans* (GenBank accession numbers BAA21847, CAA19508, CAA86773, and CAA91061), and two *Drosophila melanogaster* hect proteins (the hyperplastic disc protein and one with GenBank accession number AAD38975). The two views are related by a rotation of ~80° about the vertical axis. The view on the left has an orientation similar to that of Fig. 1A; that on the right is similar to Fig. 2. The position of the broad cleft is approximately marked by a black line. [Prepared with the program GRASP (*43*).] (**B**) Close-up view of the broad cleft. The N and C lobes of the hect domain are colored red and green, respectively. The hinge region (738 to 740) between the N and C lobes is white; the conserved side chains are yellow. The residues mutated in Angelman syndrome are indicated with white spheres. Orientation is similar to that of Fig. 1A.

References and Notes

1. M. Hochstrasser, *Annu. Rev. Genet.* **30**, 405 (1996).
2. J. D. Laney and M. Hochstrasser, *Cell* **97**, 427 (1999).
3. R. Mayer, M. Landon, J. Lowe, in *Ubiquitin and the Biology of the Cell*, J.-M. Peters, J. R. Harris, D. Finley, Eds. (Plenum, New York, 1998), pp. 429–462.
4. J. M. Huibregtse, M. Scheffner, P. M. Howley, *Mol. Cell. Biol.* **13**, 775 (1993).
5. ———, *Mol. Cell. Biol.* **13**, 4918 (1993).

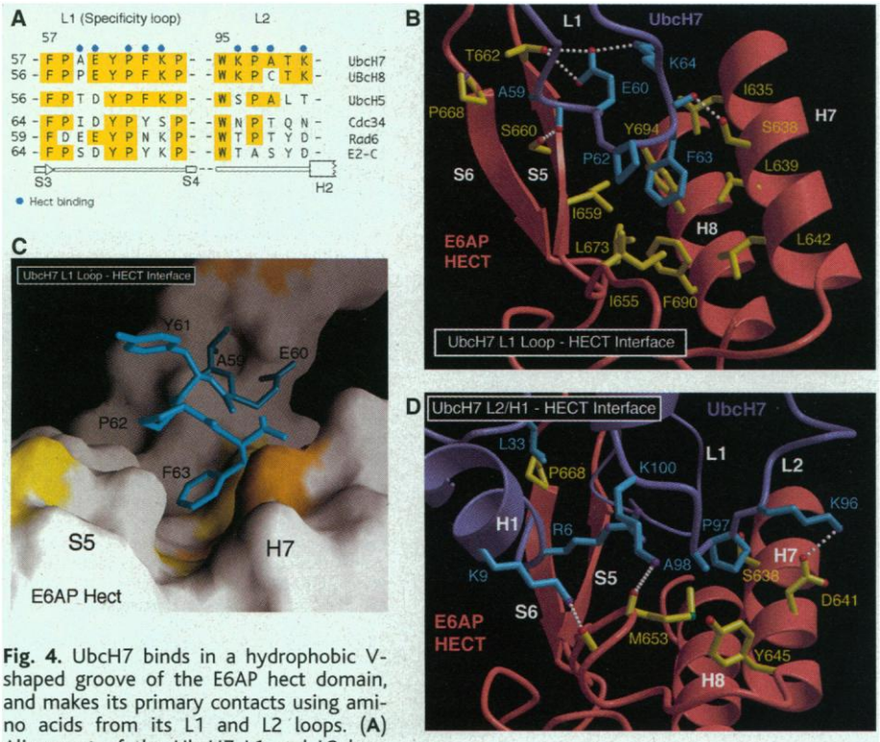

Fig. 4. UbcH7 binds in a hydrophobic V-shaped groove of the E6AP hect domain, and makes its primary contacts using amino acids from its L1 and L2 loops. (**A**) Alignment of the UbcH7 L1 and L2 loop sequences with the corresponding regions of human E2s that function with hect E3s (UbcH8 and UbcH5) or with other E3 classes. Cdc34 is the E2 in the SCF complex; Rad6, the E2 for Ubr1; and E2-C, an APC E2. Residues that are identical to residues in UbcH7 are colored yellow. Cyan dots indicate residues in UbcH7 contacting the E6AP hect. (**B**) Close-up view of a portion of the intermolecular interface between the L1 specificity loop of UbcH7 and E6AP. The interacting secondary structures of the hect domain and UbcH7 are colored red and blue, respectively, and their side chains are yellow and cyan, respectively. The L2 loop and H1 helix of UbcH7 would be immediately in front of the L1 loop, and are not shown here for clarity; they are shown in (D). (**C**) Surface representation of the E6AP hydrophobic groove, highlighting the snug fit of the UbcH7 Phe^{63} in the deepest portion of the hect groove. The surface is colored according to sequence conservation as in Fig. 3A. The residues in the L1 specificity loop of UbcH7 that interact with this surface are cyan. View is similar to that in (B). (**D**) Close-up view of a portion of the intermolecular interface between the L2 loop and H1 helix of UbcH7 and E6AP. Orientation is similar to that of (B). The L1 loop, which is behind the L2 loop in this view, is shown as a thin trace. Coloring and labeling scheme are the same as in (B). The NH_2-terminus of the UbcH7 H1 helix has high temperature factors in the refined structure; the first three residues of UbcH7 are disordered. Also shown is the UbcH7 Leu^{33}, which makes a van der Waals contact to the E6AP Pro^{668}. Leu^{33} occurs in a loop (residues 28 to 33) that does not contribute any other contacts.

6. T. Kishino, M. Lalande, J. Wagstaff, *Nature Genet.* **15**, 70 (1997); U. Albrecht *et al.*, *Nature Genet.* **17**, 75 (1997).
7. Y. Jiang, E. Lev-Lehman, J. Bressler, T. F. Tsai, A. L. Beaudet, *Am. J. Hum. Genet.* **65**, 1 (1999).
8. H. Oda, S. Kumar, P. M. Howley, *Proc. Natl. Acad. Sci. U.S.A.* **96**, 9557 (1999).
9. S. Kumar, A. L. Talis, P. M. Howley, *J. Biol. Chem.* **274**, 18785 (1999).
10. C. Kuhne and L. Banks, *J. Biol. Chem.* **273**, 34302 (1998).
11. A. L. Talis, J. M. Huibregtse, P. M. Howley, *J. Biol. Chem.* **273**, 6439 (1998).
12. M. Scheffner, S. Smith, S. Jentsch, in *Ubiquitin and the Biology of the Cell*, J.-M. Peters, J. R. Harris, D. Finley, Eds. (Plenum, New York, 1998), pp. 65–98.
13. S. E. Schwarz, J. L. Rosa, M. Scheffner, *J. Biol. Chem.* **273**, 12148 (1998).
14. M. Scheffner, U. Nuber, J. M. Huibregtse, *Nature* **373**, 81 (1995).
15. G. Wang, J. Yang, J. M. Huibregtse, *Mol. Cell. Biol.* **19**, 342 (1999).
16. S. Jentsch, *Annu. Rev. Genet.* **26**, 179 (1992).
17. U. Nuber, S. Schwarz, P. Kaiser, R. Schneider, M. Scheffner, *J. Biol. Chem.* **271**, 2795 (1996).
18. M. Scheffner, J. M. Huibregtse, P. M. Howley, *Proc. Natl. Acad. Sci. U.S.A.* **91**, 8797 (1994).
19. S. Kumar, W. H. Kao, P. M. Howley, *J. Biol. Chem.* **272**, 13548 (1997).

20. The hect domain of human E6AP [residues 495 to 852 of isoform I (*37*)] and human UbcH7 were overexpressed using the pGEX4T-3 and pET vectors, respectively, at 25°C. The hect domain fused to glutathione S-transferase (GST) was purified using a glutathione-Sepharose 4B-column (Pharmacia), cleaved with thrombin at 4°C overnight, and was further purified by anion exchange and gel filtration chromatography. UbcH7 was purified through anion exchange, cation exchange, and gel filtration chromatography. Both proteins were concentrated to 30 mg/ml by ultrafiltration in 50 mM Hepes-Na, 200 mM NaCl, and 5 mM dithiothreitol (DTT) (pH 7.4). Mass spectroscopic analyses indicated that UbcH7 retained the NH_2-terminal Met.
21. Crystals of the hect domain were grown by the hanging-drop vapor diffusion method from 11 to 12% (w/v) polyethylene glycol, molecular weight 1500 (PEG 1500), 1.92 M ammonium acetate, 0.3 M sodium chloride, 0.1 M Hepes-Na, and 5 mM DTT (pH 7.5). Crystals of the selenomethionine-substituted hect domain were grown similarly, from 14 to 15% (w/v) PEG 1500 and 0.96 M ammonium acetate. Crystals formed in space group $P2_12_12_1$, with a = 101.5 Å, b = 113.7 Å, c = 125.2 Å, and contain three hect domains in the asymmetric unit. Screening for derivatives was hampered by the high level of nonisomorphism of heavy atom–soaked crystals. This problem was partially circumvented by soaking the crystals first in 0.5 mM thimerosal, followed by either 3 mM potassium gold chloride or 5 mM mercuric chloride (L. Huang, E. Kinnucan, N. P. Pavletich, data not shown). Low-resolution multiple isomorphous replacement (MIR) phases calculated from these mercury and gold derivatives using the thimerosal-soaked crystal as the native allowed determination of the proper threefold noncrystallographic symmetry. The multiple-wavelength anomalous diffraction (MAD) data (Table 1) were obtained at the BNL X4A beamline with a selenomethionine-substituted crystal that was soaked in 1 mM thimerosal for 24 hours and flash-frozen at −160°C in crystallization buffer supplemented with 25% ethylene glycol. All data were collected at −160°C and were processed with DENZO and SCALEPACK (*38*). 27 of the 36 Se sites were identified by anomalous difference Fourier methods using the threefold averaged low-resolution MIR phases. MAD phases calculated with the program MLPHARE (*39*) had a mean figure of merit of 0.53 to 3.3 Å resolution, and were improved by solvent flattening with the program DM (*39*). The MAD electron density map had clear density for residues 497 to 850, but no density for residues 495 and 496 and residues 851 and 852, at the NH_2- and COOH-termini, respectively. The model was built into the electron density map with O (*40*) and was refined against the 2.8 Å native data set with the program CNS (*41*) (Table 1).
22. The crystals of the complex were obtained by co-crystallization of the E6AP hect domain and UbcH7, at a molar ratio of 1:1 and total protein concentration of 32 mg/ml, by the hanging-drop vapor diffusion method from 10% (w/v) PEG 1500, 0.2 M magnesium chloride, and 0.1 M Mes-Na (pH 6.5). Crystals formed in space group $P2_12_12_1$, with a = 103.4 Å, b = 112.7 Å, c = 123.8 Å, which is the same space group with closely related unit cell parameters as the hect domain–alone crystals. They contain the same trimeric form of the hect domain, and only one of the hect domains is bound by UbcH7. The UbcH7-binding site of a second hect domain is involved in crystal-packing contacts, and that of a third hect domain has little space for UbcH7 owing to crystal packing. This stoichiometry is consistent with that obtained by running extensively washed crystals in an SDS gel. The crystals of the complex were flash-frozen in crystallization buffer supplemented with 35% (v/v) ethylene glycol. The structure of the hect domain in the complex was located by molecular replacement with the program AMORE (*39*). Difference Fourier maps had clear electron density for the portion of UbcH7 that binds the hect domain. The UbcH7 structure was built using the Ubc4 structure (*23*) as a guide, and the structure of the complex was refined at 2.6 Å (Table 1) with the program CNS (*41*). The refined model contains residues 4 to 147 of UbcH7; residues 1 to 3 and 148 to 154 have no clear electron density. In the crystals, UbcH7 makes only a small number of crystal-packing contacts, and the portion of the UbcH7 structure distal from the hect-interacting portion has high temperature factors in the refined model.

23. W. J. Cook, P. D. Martin, B. F. Edwards, R. K. Yamazaki, V. Chau, *Biochemistry* **36**, 1621 (1997); W. J. Cook, L. C. Jeffrey, M. L. Sullivan, R. D. Vierstra, *J. Biol. Chem.* **267**, 15116 (1992); W. J. Cook, L. C. Jeffrey, Y. Xu, V. Chau, *Biochemistry* **32**, 13809 (1993); F. Jiang and R. Basavappa, *Biochemistry* **38**, 6471 (1999); D. K. Worthylake, S. Prakash, L. Prakash, C. P. Hill, *J. Biol. Chem.* **273**, 6271 (1998); H. Tong, G. Hateboer, A. Perrakis, R. Bernards, T. K. Sixma, *J. Biol. Chem.* **272**, 21381 (1997).
24. U. Nuber and M. Scheffner, *J. Biol. Chem.* **274**, 7576 (1999).

25. The E6AP hect domain crystallized as the same symmetric trimer in two different crystal forms (trigonal

crystal form; L. Huang, E. Kinnucan, N. P. Pavletich, data not shown) and in the E6AP-UbcH7 complex. However, the E6AP hect domain is a monomer in solution, and mutation of a residue (Phe^{727}) making key trimer contacts has little effect on the ubiquitin-thioester bond formation (L. Huang, E. Kinnucan, G. Wang, S. Beaudenon, J. M. Huibregtse, N. P. Pavletich, data not shown). The interactions associated with the formation of the trimer could, in principle, have favored the crystallization of the E6AP-UbcH7 complex in the same E6AP conformation as in the E6AP-alone crystals.

26. Equivalent amounts of purified wild-type and mutant GST-hect proteins were used in an in vitro ubiquitin-thioester assay (*14*). The reactions contained purified baculovirus-expressed human E1 protein, purified UbcH7, ^{32}P-labeled ubiquitin, and ATP. Reactions were incubated at room temperature for 5 to 10 min and stopped with SDS–polyacrylamide gel electrophoresis (PAGE) loading buffer lacking reducing agent. Products were analyzed by SDS-PAGE and autoradiography and quantified with a Molecular Dynamics Phosphoimager. The amounts of ubiquitin-thioester bond formation for the mutants, relative to the wild-type protein, are 0% for C820S, 4% for H818A, 26% for T819A, 31% for F821A, 28% for N822A, 8% for R506A, 7% for E539A, 6% for E550A, and 10% for D607A. Each reaction was repeated three times, with typical error bars of up to 4% of the wild-type activity.
27. J. M. Huibregtse, M. Scheffner, S. Beaudenon, P. M. Howley, *Proc. Natl. Acad. Sci. U.S.A.* **92**, 2563 (1995).
28. J. Clayton-Smith and S. Ramsden, personal communication.
29. P. Fang *et al.*, *Hum. Mol. Genet.* **8**, 129 (1999).
30. P. Malzac *et al.*, *Am. J. Hum. Genet.* **62**, 1353 (1998).
31. J. Wagstaff, personal communication.
32. Z. Nawaz *et al.*, *Mol. Cell. Biol.* **19**, 1182 (1999).
33. On the UbcH7 L1 loop, the Phe^{63} side chain makes van der Waals contacts with the E6AP Leu^{635}, Leu^{639}, Leu^{642}, Phe^{690}, Tyr^{694}, and Ile^{655}; the charged residues of L1, Glu^{60} and Lys^{64}, form hydrogen bonds with each other and with Gln^{661} and Thr^{662} of E6AP in the solvent-exposed end of the E6AP groove.
34. On the UbcH7 L2 loop, Pro^{97} makes van der Waals contacts with Met^{653}, Asp^{641}, and Ser^{638} of E6AP; Ala^{98} makes van der Waals contacts with Met^{653} and Tyr^{645} of E6AP; Lys^{96} forms hydrogen bonds with Asp^{641}; and Lys^{100} forms hydrogen bonds with the backbone carbonyl of Asp^{652}. The H1 helix of UbcH7 contributes minor contacts; its Arg^{6} and Lys^{9} side chains, which have high temperature factors, are within hydrogen-bonding distance of the backbone carbonyl groups of Met^{653} and Asp^{651} of E6AP, respectively. The UbcH7 Leu^{33}, which occurs in a loop (residues 28 to 33) adjacent to the H1 helix, makes a van der Waals contact to the E6AP Pro^{668}.
35. S. C. Johnston, S. M. Riddle, R. E. Cohen, C. P. Hill, *EMBO J.* **18**, 3877 (1999).
36. R. Beal, Q. Deveraux, G. Xia, M. Rechsteiner, C. Pickart, *Proc. Natl. Acad. Sci. U.S.A.* **93**, 861 (1996).
37. Y. Yamamoto, J. M. Huibregtse, P. M. Howley, *Genomics* **41**, 263 (1997).
38. Z. Otwinowski and W. Minor, *Methods Enzymol.* **276**, 307 (1997).
39. CCP4, *Acta Crystallogr.* **D50**, 760 (1994).
40. T. A. Jones, J.-Y. Zou, S. W. Cowan, M. Kjeldgaard, *Acta Crystallogr.* **A47**, 110 (1991).
41. A. T. Brünger *et al.*, *Acta Crystallogr.* **D54**, 905 (1998).
42. P. J. Kraulis, *J. Appl. Crystallogr.* **24**, 946 (1991); D. Bacon and W. F. Anderson, *J. Mol. Graphics* **6**, 219 (1988).
43. A. Nicholls, K. A. Sharp, B. Honig, *Proteins Struct. Funct. Genet.* **11**, 281 (1991).
44. Supported by NIH, the Howard Hughes Medical Institute, the Dewitt Wallace Foundation, the Samuel and May Rudin Foundation, and a Norman and Rosita Winston Foundation fellowship (L.H.). We thank J. Wagstaff at Boston Children's Hospital and S. Ramsden and J. Clayton-Smith at St. Mary's Hospital for the AS mutation data before publication; M. Scheffener for the UbcH7 plasmid; H. Erdjument-Bromage of the Sloan-Kettering Microchemistry Facility for NH_2-terminal sequence analysis; C. Ogata of the National Synchrotron Light Source (NSLS) X4A beamline, M. Sullivan of the NSLS X9B beamline, and T. Earnest, G. McDermott, K. Henderson, and L. Hung at the Advanced Light Source Beamline 5.0.2 for help with data collection; P. Jeffrey for help with synchrotron data collection; and C. Murray for administrative assistance. Coordinates have been deposited with the Protein Data Bank (accession codes 1D5F for E6AP and 1C4Z for the E6AP-UbcH7 complex).

15 September 1999; accepted 12 October 1999

Evidence for a Ubiquitous Seismic Discontinuity at the Base of the Mantle

Igor Sidorin, Michael Gurnis,* Don V. Helmberger

A sharp discontinuity at the base of Earth's mantle has been suggested from seismic waveform studies; the observed travel time and amplitude variations have been interpreted as changes in the depth of a spatially intermittent discontinuity. Most of the observed variations in travel times and the spatial intermittance of the seismic triplication can be reproduced by a ubiquitous first-order discontinuity superimposed on global seismic velocity structure derived from tomography. The observations can be modeled by a solid-solid phase transition that has a 200-kilometer elevation above the core-mantle boundary under adiabatic temperatures and a Clapeyron slope of about 6 megapascal per kelvin.

Seismic studies provide information about the composition, state, and dynamics of Earth's mantle. Global seismic velocity images represent snapshots of mantle convection (*1*), whereas more detailed waveform studies provide evidence for phase transitions, chemical heterogeneity, and partial melting in the mantle (*2–4*). Unfortunately, the interpretation of the structural features of the mantle inferred from seismology is plagued by trade-offs and ambiguities. Most global tomographic inversions do not incorporate seismic discontinuities in the mantle, attributing any associated travel time anomalies to volumetric heterogeneity. Similarly, most waveform modeling uses globally averaged one-dimensional (1D) seismic velocity reference models focusing on isolated regions without consideration of the geographical variations in velocity. This difference between seismic inversion techniques makes it difficult to distinguish localized structure from broader anomalies distributed along the ray paths. As a result, there is poor understanding of the relation between large-scale mantle convection imaged by seismic tomography and the smaller scale processes, which may include chemical heterogeneity, solid-solid phase transitions, and partial melting. The smaller scale processes produce specific signatures in the fine-scale seismic velocity field that is usually explored by waveform modeling.

One such mantle feature is a travel time triplication attributed to a sharp (*5*), 2 to 3% velocity discontinuity about 250 km above the core-mantle boundary (CMB) (*6*). The primary evidence for the triplication is an additional phase, *Scd*, arriving between the direct, *S*, and core-reflected, *ScS*, shear wave phases in about 65° to 83° distance range (*2, 7–9*). The relative timing and amplitudes of the three phases experience significant regional variations. This intermittent triplication may be due to a laterally varying D″ discontinuity (*10*). Alternatively, the observed spatial intermittance of the triplication may be attributed to variations of the local velocity gradients accompanying a small (≈1%) velocity jump (*11*).

The triplication is strong or detectable beneath the circum-Pacific region, which has been associated with zones of faster-than-average velocities at the base of the mantle (Fig. 1), and it is weak or undetectable in anomalously slow regions (*12*). This suggests that the local structure can modulate the strength of the triplication produced by a possibly ubiquitous discontinuity. This poses the question if it is possible to predict the observed geographic patterns in the strength and timing of the phases associated with the triplication by using the structure inferred by tomographic inversions.

We used Grand's shear wave velocity

Seismological Laboratory 252-21, California Institute of Technology, Pasadena, CA 91125, USA.

*To whom correspondence should be addressed. E-mail: gurnis@caltech.edu

References and Notes

[8] **Regulation of the Src Family Tyrosine Kinase Blk through E6AP-Mediated Ubiquitination**

Hideaki Oda; Sushant Kumar; Peter M. Howley

Proceedings of the National Academy of Sciences of the United States of America, Vol. 96, No. 17. (Aug. 17, 1999), pp. 9557-9562.

Stable URL:

http://links.jstor.org/sici?sici=0027-8424%2819990817%2996%3A17%3C9557%3AROTSFT%3E2.0.CO%3B2-P

[18] **Identification of a Human Ubiquitin-Conjugating Enzyme that Mediates the E6-AP-Dependent Ubiquitination of p53**

Martin Scheffner; Jon M. Huibregtse; Peter M. Howley

Proceedings of the National Academy of Sciences of the United States of America, Vol. 91, No. 19. (Sep. 13, 1994), pp. 8797-8801.

Stable URL:

http://links.jstor.org/sici?sici=0027-8424%2819940913%2991%3A19%3C8797%3AIOAHUE%3E2.0.CO%3B2-H

[27] **A Family of Proteins Structurally and Functionally Related to the E6-AP Ubiquitin-Protein Ligase**

Jon M. Huibregtse; Martin Scheffner; Sylvie Beaudenon; Peter M. Howley

Proceedings of the National Academy of Sciences of the United States of America, Vol. 92, No. 7. (Mar. 28, 1995), pp. 2563-2567.

Stable URL:

http://links.jstor.org/sici?sici=0027-8424%2819950328%2992%3A7%3C2563%3AAFOPSA%3E2.0.CO%3B2-9

LINKED CITATIONS

[36] **Surface Hydrophobic Residues of Multiubiquitin Chains Essential for Proteolytic Targeting**
Richard Beal; Quinn Deveraux; Gang Xia; Martin Rechsteiner; Cecile Pickart
Proceedings of the National Academy of Sciences of the United States of America, Vol. 93, No. 2. (Jan. 23, 1996), pp. 861-866.
Stable URL:
http://links.jstor.org/sici?sici=0027-8424%2819960123%2993%3A2%3C861%3ASHROMC%3E2.0.CO%3B2-B